Nucleophilic Substitution Reaction Based Layer-by-Layer Growth of Superparamagnetic Nanocomposite Films with High Nonvolatile Memory Performance

By *Younghoon Kim, Chanwoo Lee, Inbo Shim, Dayang Wang,* and *Jinhan Cho**

It is very important to embed superparamagnetic nanoparticles (SPM_{NPs}) in nonmagnetic polymer matrices for a range of technical applications, such as data storage and in vivo magnetic manipulation in biomedical systems.[1] Two important factors must be considered for the preparation of such nanocomposite films. First, the SPM_{NPs} should be of good quality, including uniform size and high crystallinity. From the point of view of material preparation, the synthesis of SPM_{NPs} in organic media via thermal pyrolysis[2] is more desirable than synthesis in aqueous media.[3] Second, a uniform dispersion of a large amount of SPM_{NPs} into polymer matrices is needed. The long alkane chain-capped SPM_{NPs} obtained by organic synthesis approaches are quite compatible with hydrophobic polymer matrices, which allow a uniform dispersion of the SPM_{NPs}. However, the SPM_{NP} concentration in the polymer matrices is low, and an increase in particle concentration usually leads to aggregates with dimensions of several hundreds of nanometers due to thermodynamically unfavorable interactions.[4]

Layer-by-layer (LbL) assembly based on complementary interactions provides a versatile and simple way of fabricating nanocomposite films with tailored functionality and nanostructures as well as controlled film thickness on the nanoscale.[5] Kotov et al. fabricated nanocomposite multilayered films via electrostatic LbL assembly between negatively charged magnetite nanoparticles synthesized directly in aqueous media and polyelectrolytes. In addition, they demonstrated a strong dependence of the magnetic properties of the multilayers on the multilayer architecture.[6] However, aqueous nanoparticles are of poorer quality than organic ones, and the electrostatic repulsion between nanoparticles of the same charge considerably reduces the packing density of each SPM_{NP} layer (by 30%). Therefore, the electric, magnetic and photonic performance of nanocomposite films obtained via electrostatic LbL assembly is poor.[7] LbL assembly has been implemented successfully in polar organic solvents to increase the packing density of nanoparticles.[8] However, both strategies using LbL assembly in aqueous and polar organic solvents cannot be applied directly to grow data storage devices due to the undesired leakage current from the residual or diffused moisture. In these cases, thermal treatment is needed. Recently, we successfully developed an LbL assembly based on a nucleophilic substitution (NS) reaction between amino and bromo groups, which allows the growth of nanocomposite multilayered films in organic solvents, particularly nonpolar solvents such as toluene, and delivers a maximal packing density of randomly close-packed nanoparticles for each layer.[9]

In this study, Fe_3O_4 SPM_{NP}/poly(amidoamine) dendrimer (PAMA) nanocomposite multilayered films were successfully generated via nucleophilic substitution-based LbL assembly in organic solvents. These films showed highly improved magnetic properties compared to those obtained by electrostatic LbL assembly. Of particular importance, the resulting nanocomposite multilayered films showed better nonvolatile resistive switching memory (NRSM) performance without an additional process (i.e., thermal treatment) after multilayer preparation, including a large current ON/OFF ratio of ~10^3, operating voltage <1.5 V, rapid switching speed on the nanosecond level and long-term stability in air. There is considerable difficulty in utilizing nanocomposite multilayered films obtained via conventional LbL assembly for NRSM because of the lower packing density of active nanoparticles and the leakage current due to the presence of moisture. NRSM devices are essential for mobile electronics, such as MP3 players, digital cameras and mobile telephones. Currently, NRSM devices are derived from vacuum deposition or sol-gel chemistry (requiring thermal treatment at >200 °C) of transition metal oxides, such as TiO_2, LiO and ZnO.[10] In contrast, the approach proposed in this study is simple and cheap, as it only consists of a solution dipping process under air. This process is very important in that our approach can be effectively applied to the flexible nonvolatile memory devices using plastic substrates. The device performance of the resulting nanocomposite films was found to be comparable to that of transition metal oxide films produced by conventional vacuum deposition or sol-gel processes. Although we for the first time reported that LbL multilayers containing

[*] Y. Kim,[+] Prof. J. Cho
Department of Chemical and Biological Engineering
Korea University
Anam-dong, Seongbuk-gu, Seoul, 136–701 (Korea)
E-mail: jinhan71@korea.ac.kr
C. Lee[+]
School of Advanced Materials Engineering
Kookmin University
Jeongneung-dong, Seongbuk-gu, Seoul, 136–702 (Korea)
Prof. I. Shim
Department of Nano and Electronic Physics
Kookmin University
Jeongneung-dong, Seongbuk-gu, Seoul, 136–702 (Korea)
Prof. D. Wang
Ian Wark Research Institute
University of South Australia
Adelaide, SA 5095 (Australia)
[+] These authors contributed equally to this work

DOI: 10.1002/adma.201002142

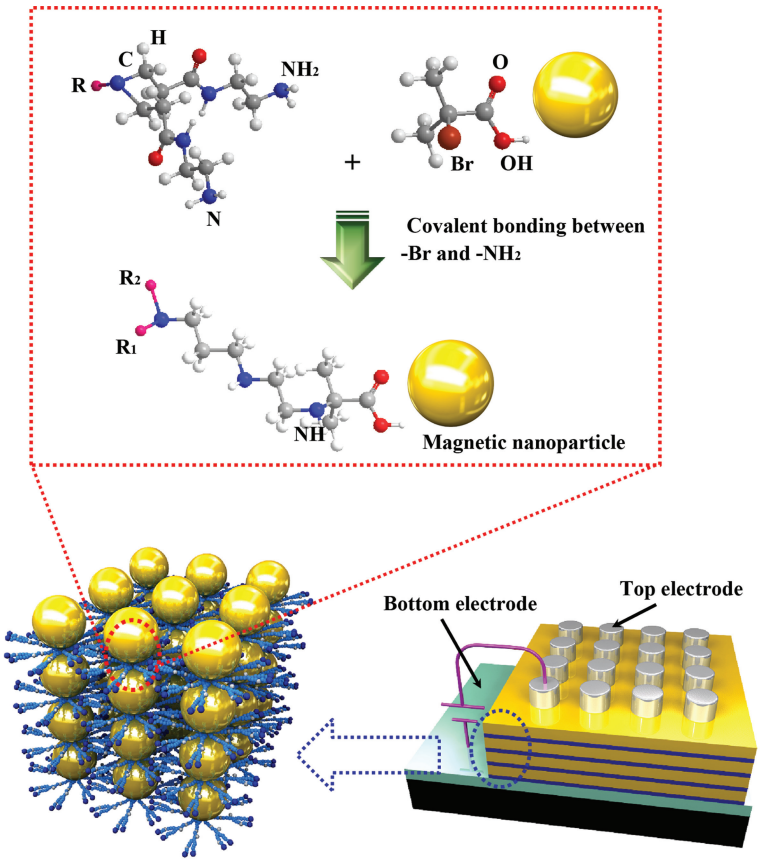

Scheme 1. Schematic representation of LbL growth of PAMA/BMPA-SPM_{NP} multilayer films based on NS reaction with the set-up for assessment of NRSM performance.

metal nanoparticles can be used as charge-trap flash memory devices, these devices have the operation system and physics quite differnet from NRSM devices.[11]

Fe_3O_4 SPM_{NPs} stabilized by 2-bromo-2-methylpropionic acid (BMPA) (i.e., BMPA-SPM_{NP}) were prepared by the ligand exchange of BMPA on oleic acid-stabilized Fe_3O_4 (see Supporting Information, Figure S1). According to a previous protocol,[9] BMPA-SPM_{NPs} and highly branched PAMAs were deposited alternatively on planar substrates using NS between bromo groups of the BMPAs on the SPM_{NPs} and the amino groups of the PAMAs (**Scheme 1**). The NS reaction was confirmed by Fourier transform infrared spectroscopy (FTIR) (Figure S2). The LbL assembly of BMPA-SPM_{NP} and PAMA was monitored by UV-vis spectroscopy. The intensity of the absorbance peak at 250 nm (due to BMPA-SPM_{NP}) increased linearly with increasing layer number, suggesting a regular amount of BMPA-SPM_{NP} adsorption per bilayer (**Figure 1a**). The amounts of PAMAs and BMPA-SPM_{NPs} adsorbed on the multilayer films were quantified by quartz crystal microgravimetry (QCM) (Figure 1b) (see the detailed methods in the Supporting Information). In addition, the SPM_{NPs} layer formed by NS in nonpolar solvent was an average monolayer with high packing density and partly aggregated particles and was very similar to those resulting from electrostatic LbL assembly of charged nanoparticles with a decreased electrostatic repulsion between neighboring nanoparticles (Figure S3).

Cross-sections of PAMA/BMPA-SPM_{NP} multilayered films were measured by scanning electron microscopy (SEM), and the film thicknesses were approximately 45 nm, 77 nm and 110 nm for 5, 10 and 15 layers, respectively (Figure 1c). The adsorbed amounts of the PAMA/BMPA-SPM_{NP} bilayer films and their morphology were examined as a function of the adsorption time. The amount of BMPA-SPM_{NPs} adsorbed onto the dendrimer layer followed the typical adsorption isotherm for LbL assembly (Figure S4a).[12] A homogeneous distribution of SPM_{NPs} on a length scale of 200 nm was observed after 30 min of adsorption (Figure S4b). A further increase in the adsorption time (e.g., 50 min) caused <10% variation in the numerical density of the SPM_{NPs} adsorbed in the defined area of 200 × 200 nm^2. These results suggest that the nonspecific adsorption of additional BMPA-SPM_{NPs} (i.e., not occurring via NS reaction) was efficiently screened.

The magnetization of the resulting PAMA/BMPA-SPM_{NP} films was examined by superconducting quantum interference device magnetometry (SQUID). The magnetization curves of the multilayered films measured at room temperature (T = 298 K) were reversible without coercivity, remanence or hysteresis, suggesting typical superparamagnetic behavior. This was also confirmed in the magnetization recorded in minute intervals in a low applied field (Figure S5). At liquid helium temperature (T = 5 K), the thermally activated magnetization flipping properties of the SPM_{NPs} revealed frustrated superparamagnetic properties. The magnetization curves acquired a loop shape with distinct separation of the two sweeping directions typically observed with ferromagnets (Figure S6). The saturated magnetization increased regularly with increasing bilayer number and with the total amount of BMPA-SPM_{NPs} adsorbed within the multilayer films (**Figure 2a**). The magnetization per gram of adsorbed nanoparticles was similar for different multilayered films and showed a saturated magnetism of approximately 90 $emu \cdot g^{-1}$ with negligible discrepancy (Figure 2b). Therefore, the magnetic coupling of the resulting PAMA/BMPA-SPM_{NP} films was strongly dependent on the short-range electron exchange and long-range magnetostatic interactions between the neighboring SPM_{NPs} in the lateral direction rather than the vertical direction. The organic spacers including both the PAMA layers and BMPA coating were sufficient to prevent exchange interactions between adjacent SPM_{NP} layers. Furthermore, the saturated magnetism values per gram shown in Figure 2b were significantly higher than those of iron oxide-based multilayers reported elsewhere.[13] The magnetic anisotropy constant (K) is the energy required to change the magnetization direction of two- and three-dimensional SPM_{NPs} ($K = 25\ k_B \cdot T_B \cdot V^{-1}$, where k_B is Boltzmann's constant, T_B is the blocking temperature and V is the volume of a single SPM_{NP}). The measured K was 4.58×10^5 $erg \cdot cm^{-3}$. Figure 2c shows the temperature dependence of the magnetization of the resulting PAMA/BMPA-SPM_{NP} films from 300 K to 5 K under an applied magnetic field of 150 Oe. The blocking temperature,[14] which began to show some deviation between zero-field-cooling (ZFC) and

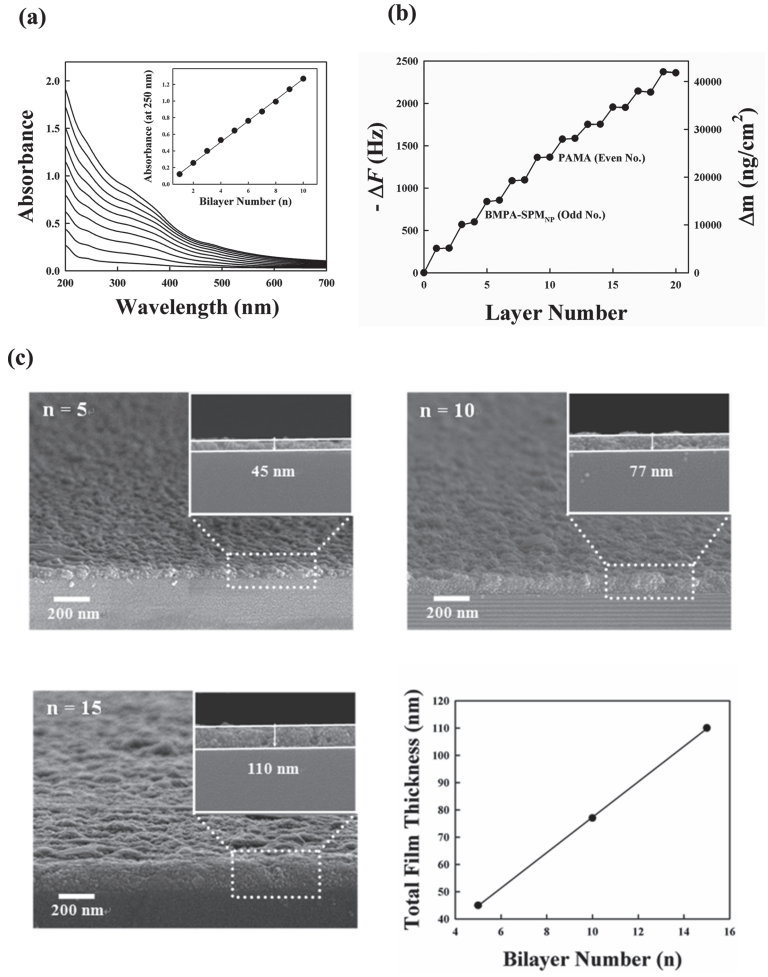

Figure 1. (a) UV-vis spectra, (b) QCM data and (c) cross-sectional SEM images of PAMA/BMPA-SPM_{NP} multilayers as a function of the layer number, respectively. The inset of (a) indicates the absorbance measured at 250 nm as a function of bilayer number.

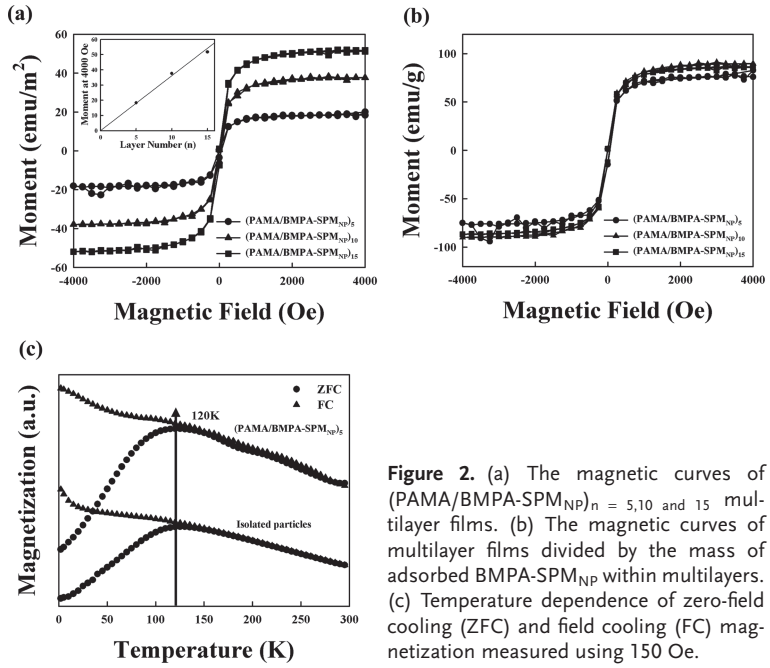

Figure 2. (a) The magnetic curves of $(PAMA/BMPA\text{-}SPM_{NP})_{n\ =\ 5,10\ and\ 15}$ multilayer films. (b) The magnetic curves of multilayer films divided by the mass of adsorbed BMPA-SPM_{NP} within multilayers. (c) Temperature dependence of zero-field cooling (ZFC) and field cooling (FC) magnetization measured using 150 Oe.

field-cooling (FC) magnetization, was fixed at approximately 120 K for both isolated nanoparticles and multilayered films, suggesting that the unique magnetic properties (i.e., magnetic anisotropic constant) of isolated SPM_{NPs} can be maintained in a 3D array. It has been reported that the blocking temperature of an Fe_3O_4 nanoparticle array was largely shifted to higher temperatures upon changing from an isolated to a 3D nanoparticle array due to relatively strong dipolar interactions between the magnetic moments of individual particles.[15] In this case, the Langmuir-Blodgett method was used for the build up of nanoparticle multilayers without the aid of insulating polymers. On the other hand, the PAMA/BMPA-SPM_{NP} multilayers in our approach could preserve the intrinsic magnetic properties of isolated nanoparticles because the inserted dendrimer layer and BMPA stabilizers can effectively screen the dipolar interactions between magnetic nanoparticles.

It was reported by Kim et al. that Fe_3O_4 nanoparticles below 10 nm in size, without any organic components including surface stabilizers, were pressed into compact pellets and the resulting nanoparticle pellets showed relatively high resistivity (>50 MΩ·cm) due to the nanosize effect.[16a] Although they suggested that the nanoparticle pellets exhibited bipolar resistive switching properties depending on the voltage polarity, their results were strongly caused by the faulty fluctuation from the measurement instrument.[16b] **Figure 3** shows the NRSM properties of the PAMA/BMPA-SPM_{NP} films. The BMPA-SPM_{NPs} used were approximately 7 nm in diameter size and their T_B was approximately 40 K (Figure S7) due to the smaller dimensions.[2a] For measurement of bipolar switching, the voltage was swept from 0 V to –1.5 V and then back to +1.5 V with limited current compliance up to 100 mA. As shown in Figure 3a, the low current state, that is, OFF state [step '(1)'], was suddenly converted to a high current state, that is, ON state, at –1.5 V when the polarity of the voltage applied to the PAMA/BMPA-SPM_{NP} films was reversed (step '(2)'). The increase in the layer number largely decreased the current level, mainly the OFF current level, because the electric field across the PAMA/BMPA-SPM_{NP} films decreased with increasing film thickness (Figure 3a and Figure S8). Figure 3b shows that the ON and OFF states remained stable during the entire test period of 10^5 s and the cycling test of 200 times under ambient conditions. The ratio of the current in the ON state to that in the OFF state was ~10^3, and these devices were operated repeatedly at switching speeds ranging from 100 ns to 1 μs (Figure 3c and Figure S9). These reversible switching properties and large ON/OFF ratios were maintained for up to one year (Figure S10), demonstrating excellent electrical stability with a rapid switching speed. This electrical stability is strongly influenced by the hydrophobic properties of multilayered devices and the thermally stable inorganic nanoparticles (Figure S11).

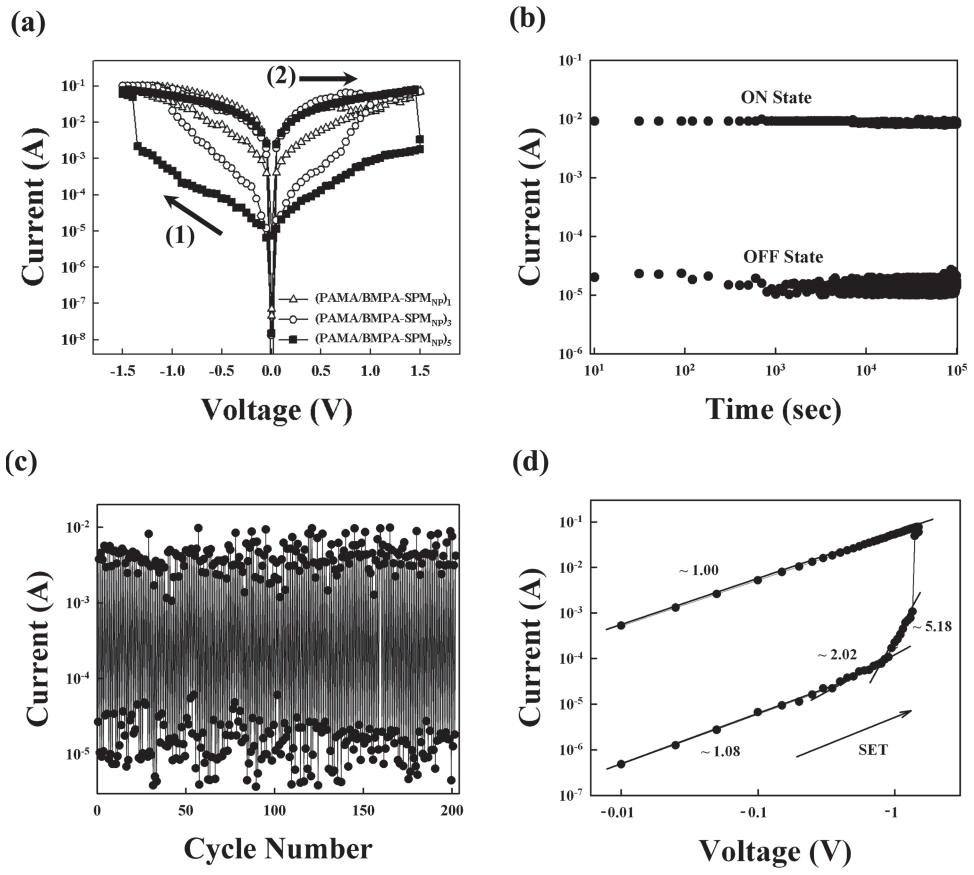

Figure 3. (a) *I–V* curves of (PAMA/7 nm-sized BMPA-SPM$_{NP}$)$_n$ multilayer devices with increasing bilayer number (n) from 1 to 5. (b) Retention time test of (PAMA/BMPA-SPM$_{NP}$)$_5$ multilayer device at a reading voltage of 0.1 V. (c) The cycling tests of 5 bilayered devices measured at a switching speed of 100 ns. (d) The linear fitting for the *I–V* curve of 5 bilayered devices on a log-log scale during a negative voltage sweep ['(1)' → '(2)'].

To understand the conducting behavior of the PAMA/BMPA-SPM$_{NP}$ films, the nonlinear *I–V* characteristics in the negative voltage sweep region were plotted on a log-log scale. Figure 3d shows that the *I–V* relationship in the ON state clearly had Ohmic conduction behavior with a slope of 1.00, which was attributed to the formation of conducting paths in the device during the SET process. However, the conducting behavior in the OFF state was much more complicated. The fitting results for the OFF state showed similar charge transport behavior to space charge limited conduction (SCLC), which consists of three different regions: an Ohmic region ($I \propto V$), a Child's law region ($I \propto V^2$) and a sharp current increase region.[17,18] The totally different conduction behavior in the ON and OFF states also suggests that the high conductivity in the ON-state device was a localized conducting effect rather than a homogeneously distributed one.

Although the switching mechanism in NRSM devices is unclear, a possible mechanism for this system is proposed based on the Memristor model.[10c,e,17] A negative voltage applied to the top electrode attracts positively charged carriers (i.e., Fe^{2+} and Fe^{3+}) in the SPM$_{NP}$ lattices due to tunneling through a thin residual region (i.e., un-doped charge carrier region within the SPM$_{NPs}$ and organic layers with approximately 1 nm thickness per bilayer, including BMPA stabilizers and PAMA layers), which induces the high current state of the films. These charges flow through localized paths in the high current state (a detailed explanation of the switching mechanism is given in the Supporting Information).

The oleic acid-stabilized SPM$_{NPs}$ were transferred from toluene to aqueous media using water-dispersible octakis (8 mmol, the same concentration as that of BMPA for ligand exchange) (Figure S12a). The amount of octakis-stabilized SPM$_{NPs}$ adsorbed onto the PAMA layer at pH > 7 was measured to be about $\Delta m \sim 1767\ ng \cdot cm^{-2}$ ($\Delta F \sim 100$ Hz and a number density of $\sim 3.78 \times 10^{11} \cdot cm^{-2}$) per layer. As a result, the PAMA/octakis-SPM$_{NP}$ films showed magnetization with a rather low intensity compared to the PAMA/BMPA-SPM$_{NP}$ films (Figure S12b). The resulting films also exhibited a rather low ON/OFF current ratio of approximately 10, even after thermal treatment (120 °C for 2 hr) to remove the residual water within the films (Figure S10c). Although reduction of the surrounding pH could reduce the charge density of octakis-stabilized SPM$_{NPs}$ and increase the amount of particle adsorption, the nanoparticles tended to aggregate at pH < 7.

In summary, SPM$_{NP}$/polymer nanocomposite films were grown by LbL based on the NS reaction between the bromo and amino groups in organic solvents. The resulting films had a maximal packing density of SPM$_{NPs}$ in each particle layer, and the magnetic properties of the SPM$_{NPs}$ were well preserved in the resulting nanocomposite films, which is difficult to implement using conventional LbL assembly techniques. In particular, the resulting nanocomposite films showed excellent NRSM performance, that is, a relatively high ON/OFF current ratio of ~10^3, rapid switching speed within 100 ns, and a long-term stability of 10^5 s under air. To the best of our knowledge, this is the first report of the LbL growth of nanoparticle-based multilayered films for NRSM devices. Compared to the conventional techniques for preparing NRSM devices, this approach is simple, inexpensive, versatile and suitable for large area production.

Experimental Section

Materials: Oleic acid-stabilized Fe_3O_4 with a diameter size of 12 ± 0.9 nm and 7 ± 0.5 nm were synthesized in toluene.[2a] The ligand exchange of oleic acid with BMPA by the addition of BMPA (1.336 g,

8 mmol) to the toluene dispersions of the SPM_{NP} (40 mL) was followed by stirring at room temperature. Octakis-stabilized SPM_{NPs} were prepared using octakis (8 mmol) for the phase transfer of oleic acid Fe_3O_4 from toluene to water. In this case, 100 mg of oleic acid-SPM_{NP} were dissolved in 7.5 mL of toluene, and 750 mg of excess octakis was dissolved in pH 9 water (7.5 mL). Experimental details are given in the Supporting Information.

Supporting Information

Supporting Information is available from the Wiley Online Library or from the author.

Acknowledgements

This work was supported by KOSEF grant funded by the Korea government (MEST) (2010–0029106, 2008–0058617, 2009–0085070), the IT R&D program of MKE/KEIT (10030559, Development of next generation high performance organic/nano materials and printing process technology), and ERC Program of KOSEF grant funded by the Korea government (MEST) (R11–2005-048–00000-0). Additionally, this work was partially supported by the Korea Research Foundation Grant funded by the Korean Government (KRF-2008–2-D00264).

Received: June 10, 2010
Revised: August 9, 2010
Published online: October 13, 2010

[1] a) X. Huang, L. M. Bronstein, J. Retrum, C. Dufort, I. Tsvetkova, S. Aniagyei, G. Stucky, B. McKenna, N. Remmes, D. Baxter, C. C. Kao, B. Dragnea, *Nano Lett.* **2007**, *7*, 24070; b) J. Kim, S. Park, J. E. Lee, S. M. Jin, J. H. Lee, I. S. Lee, I. Yang, J.-S. Kim, S. K. Kim, M.-H. Cho, T. Hyeon, *Angew. Chem.Int. Ed.* **2006**, *45*, 7754; c) D. E. Speliotis, *J. Magn. Magn. Mater.* **1999**, *193*, 29; d) B.-S. Kim, J.-M. Qiu, J.-P. Wang, T. A. Taton, *Nano Lett.* **2005**, *5*, 1987.

[2] a) J. Park, K. An, Y. Hwang, J.-E. Park, H.-J. Noh, J.-Y. Kim, J.-H. Park, N.-M. Hwang, T. Hyeon, *Nat. Mater.* **2004**, *3*, 891; b) J. Rockenberger, E. C. Scher, A. P. Alivisatos, *J. Am. Chem. Soc.* **1999**, *121*, 11595.

[3] a) Z. J. Zhang, Z. L. Wang, B. C. Chakoumakos, J. S. Yin, *J. Am. Chem. Soc.* **1998**, *120*, 1800; b) S. Sun, H. Zeng, D. B. Robinson, S. Raoux, P. M. Rice, S. X. Wang, G. Li, *J. Am. Chem. Soc.* **2004**, *126*, 273.

[4] M. K. Corbierre, N. S. Cameron, M. Sutton, S. G. J. Mochrie, L. B. Lurio, A. Rühm, R. B. Lennox, *J. Am. Chem. Soc.* **2001**, *123*, 10411.

[5] a) G. Decher, *Science* **1997**, *277*, 1232; b) F. Caruso, R. A. Caruso, H. Möhwald, *Science* **1998**, *282*, 1111; c) M.-K. Park, S. Deng, R. C. Advincula, *J. Am. Chem. Soc.* **2004**, *126*, 13723; d) L. Zhai, F. C. Cebeci, R. E. Cohen, M. F. Rubner, *Nano Lett.* **2004**, *4*, 1349.

[6] a) A. A. Mamedov, N. A. Kotov, *Langmuir* **2000**, *16*, 5530; b) A. A. Mamedov, J. Ostrander, F. Aliev, N. A. Kotov, *Langmuir* **2000**, *16*, 3941.

[7] a) V. R. Hering, G. Gibson, R. I. Schumacher, A. Faljoni-Alario, M. J. Politi, *Bioconjugate Chem.* **2007**, *18*, 1705; b) F. Caruso, M. Spasova, A. Susha, M. Giersig, R. A. Caruso, *Chem. Mater.* **2001**, *13*, 109; c) W. S. Choi, H. Y. Koo, J.-H. Park, D.-Y. Kim, *J. Am. Chem. Soc.* **2005**, *127*, 16136; d) A. F. Thünemann, D. Schütt, L. Kaunfner, U. Pison, H. Möhwald, *Langmuir* **2006**, *22*, 2351.

[8] E. Hao, T. Lian, *Chem. Mater.* **2000**, *12*, 3392.

[9] B. Lee, Y. Kim, S. Lee, Y. S. Kim, D. Wang, J. Cho, *Angew. Chem. Int. Ed.* **2010**, *49*, 359.

[10] a) T. Zhang, Z. Su, H. Chen, L. Ding, W. Zhang, *Appl. Phys. Lett.* **2008**, *93*, 172104; b) R. Waser, M. Aono, *Nat. Mater.* **2007**, *6*, 833; c) D. B. Strukov, G. S. Snider, D. R. Stewart, R. S. Williams, *Nature* **2008**, *453*, 80; d) W.-Y. Chang, K.-J. Cheng, J.-M. Tsai, H.-J. Chen, F. Chen, M.-J. Tsai, T. B. Wu, *Appl. Phys. Lett.* **2009**, *95*, 042104; e) J. J. Yang, M. D. Pickett, X. Li, D. A. A. Ohlberg, D. R. Stewart, R. S. Williams, *Nat. Nanotech.* **2008**, *3*, 429; f) T. Zhang, Z. Su, H. Chen, L. Ding, W. Zhang, *Appl. Phys. Lett.* **2008**, *93*, 172104; g) C. Lee, I. Kim, H. Shin, S. Kim, J. Cho, *Langmuir* **2009**, **25**, 11276; h) C. Lee, I. Kim, W. Choi, H. Shin, J. Cho, *Langmuir* **2009**, **25**, 4274; i) C. Lee, I. Kim, H. Shin, J. Cho, *Nanotechnology* **2010**, **21**, 185704.

[11] J. S. Lee, J. Cho, C. Lee, I. Kim, J. Park, Y. Kim, H. Shin, J. Lee, F. Caruso, *Nat. Nanotechnol.* **2007**, *2*, 790.

[12] M. Raposo, O. N. Oliveira, *Langmuir* **2002**, *18*, 6866.

[13] a) X. Hong, J. Li, M. Wang, J. Xu, W. Guo, J. Li, Y. Bai, T. Li, *Chem. Mater.* **2004**, *16*, 4022; b) L. Wang, Z. Yang, Y. Zhang, L. Wang, *J. Phys. Chem. C.* **2009**, *113*, 3955.

[14] a) Y. Köseoğlu, H. Kavas, *J. Nanosci. Nanotechnol.* **2008**, *8*, 584; b) T. Ozkaya, M. S. Toprak, A. Baykal, H. Kavas, Y. Köseoğlu, B. Aktaş, *J. Alloys and Compounds* **2009**, *472*, 18.

[15] P. Poddar, T. Telem-Shafir, T. Fried, G. Markovich, *Phys. Rev. B* **2002**, *66*, 060403.

[16] a) T. H. Kim, E. Y. Jang, N. J. Lee, D. J. Choi, K.-J. Lee, J.-T. Jang, J.-S. Choi, S. H. Moon, J. Cheon, *Nano Lett.* **2009**, *9*, 2229; b) Correction: T. H. Kim, E. Y. Jang, N. J. Lee, D. J. Choi, K.-J. Lee, J.-T. Jang, J.-S. Choi, S. H. Moon, J. Cheon, *Nano Lett.* **2010**, *10*, 2734.

[17] A. Lampert, P. Mark, *Current Injection in Solids; Academic*: New York **1970**.

[18] Y. C. Yang, F. Pan, Q. Liu, M. Liu, F. Zeng, *Nano Lett.* **2009**, *9*, 1636.